Applied Physics A (2019) 125:802
https://doi.org/10.1007/s00339-019-3099-2

Applied Physics A
Materials Science & Processing

Assessment of gamma-rays and fast neutron beam attenuation features of Er_2O_3-doped B_2O_3–ZnO–Bi_2O_3 glasses using XCOM and simulation codes (MCNP5 and Geant4)

G. Lakshminarayana[1] · M. G. Dong[2] · Ashok Kumar[3] · Y. Elmahroug[4,5] · Akshatha Wagh[1] · Dong-Eun Lee[6] · Jonghun Yoon[7] · Taejoon Park[8]

Received: 27 September 2019 / Accepted: 23 October 2019 / Published online: 3 November 2019

Abstract
The authors aim to study the gamma-rays and neutron beam shielding capabilities of zinc bismuth borate glasses doped with erbium ions. Mass attenuation coefficient (MAC) (μ/ρ) values were computed employing XCOM and two different simulation codes, MCNP5 and Geant4, within 0.015–15 MeV photon energy, which showed good agreement within the derived values. The effective atomic number (Z_{eff}), electron density (N_e), half-value layer (HVL) and mean free path (MFP) values were derived using MAC values. To account on the scattering effects of photons from the samples, exposure buildup factor (EBF) were determined, applying geometric progression (G-P) method, within 0.015–15 MeV photon energy and penetration depth of 1–40 mfp (intervals: 1, 5, 10, 15, and 40 mfp). The high MAC, Z_{eff} values and low HVL, MFP values of $16.93B_2O_3$−$22.57ZnO$−$60Bi_2O_3$−$0.5Er_2O_3$ (mol%) glass optimized its shielding effects against gamma-rays. The macroscopic effective removal cross-section for fast neutron (Σ_R) values lie within the range of 0.1142–0.1232 cm^{-1} for the selected Er_2O_3-doped samples. The studied parameters of the experimented glasses revealed their dominant radiation shielding features compared to commercial shielding glasses, concretes, and alloys.

1 Introduction

Nowadays, wide use of radioactive isotopes in fields such as nuclear medicine, food irradiation, agriculture, and petroleum industry is showing encouraging outcomes. In nuclear power plants, the use of radioactive materials that emit neutron beam, X-rays and gamma-rays is mandatory. Though nuclear energy is considered as an alternative cleaner energy source, there are issues associated with the excessive radiation exposure to the workers if scattered, leaked or directly exposed, and environmental effects with radioactive waste storage. High-energetic X-rays, γ-rays, and neutrons are

✉ G. Lakshminarayana
gandham@knu.ac.kr

✉ Dong-Eun Lee
dolee@knu.ac.kr

✉ Jonghun Yoon
yooncsmd@gmail.com

✉ Taejoon Park
taejoon@hanyang.ac.kr

[1] Intelligent Construction Automation Center, Kyungpook National University, 80, Daehak-ro, Buk-gu, Daegu 41566, Republic of Korea

[2] Department of Resource and Environment, Northeastern University, Shenyang 110819, China

[3] Department of Physics, University College, Benra, Dhuri, Punjab, India

[4] Université de Tunis El Manar, Faculté des Sciences de Tunis, Unité de Recherche de Physique Nucléaire et des Hautes Energies, 2092 Tunis, Tunisia

[5] Ecole Centrale Polytechnique Privée de Tunis, Univesité Centrale, Tunis, Tunisia

[6] School of Architecture and Civil Engineering, Kyungpook National University, 80, Daehak-ro, Buk-gu, Daegu 41566, Republic of Korea

[7] Department of Mechanical Engineering, Hanyang University, 55 Hanyangdaehak-ro, Ansan, Gyeonggi-do 15588, Republic of Korea

[8] Department of Robotics Engineering, Hanyang University, 55 Hanyangdaehak-ro, Ansan, Gyeonggi-do 15588, Republic of Korea

hazardous for living cells and tissues in humans and animals and long-time exposure to highly penetrating ionizing radiations like γ-rays could cause genetic alterations, cancer, and even death. Thus, to safeguard the living beings and reduce the radiations to acceptable levels coming from the nuclear power plants, industries, research laboratories and medical departments a suitable shielding material is necessary [1–3]. Attenuating the alpha, beta, neutron beam, X-rays and γ-rays has been effectively done by concretes and lead (Pb)-based glasses at radiation therapy centers, reactors, and nuclear waste storage sites. However, concretes have drawbacks such as non-transparency to visible light or opaque nature, non-portability, loss of water content due to radiation absorption, and cracks formation with prolonged radiation exposure, whereas Pb-based glasses contain 'Pb' element, which is toxic in nature to the environment and the human health [4, 5].

Therefore, a pressing need is to develop non-toxic Pb-free glasses which shows radiation shielding characteristics for neutron and γ-rays. Generally, glasses are cost-effective, easy to fabricate in distinct shapes and sizes along with flexibility in chemical composition and optical transparency to visible light. Glasses possess better mechanical and chemical durability, and good thermal stability to investigate and explore their radiation shielding features [1, 2]. Moreover, the addition of heavy-metal oxides (HMOs) or high *Z*-materials [e.g., BaO ($Z=56$), Bi_2O_3 ($Z=83$)] to the glass composition imparts higher density and large effective atomic number (Z_{eff}). The high molecular mass and high density of the glasses absorb γ-rays and neutrons to a larger extent, increasing the probability of the interactions between incoming radiation and glass components. In recent reports, gamma-rays and neutron shielding capabilities of Pb-free glasses showed fewer hygiene concerns [1, 2, 6–10]. The probability of γ-rays' interactions with the matter is analyzed by the mass attenuation coefficient (MAC) (μ/ρ) parameter. Other photon interaction parameters such as Z_{eff}, effective electron density (N_e), half-value layer (HVL), and mean free path (MFP) can be evaluated using MAC values. The lowest values of HVL and MFP present as the best choice for radiation shielding applications [11, 12].

B_2O_3 is one of the superior glass network formers among other glass-forming oxides such as SiO_2, P_2O_5, and GeO_2. The borate glasses possess features such as low-cost fabrication, easy glass-forming ability, low melting point, low viscosity, good optical transparency, high chemical resistance, and good mechanical and thermal stability [5, 6, 10]. Here, boron (B) atom possesses high bond strength and low cation size and acts as a promising nucleon shielding element for nuclear waste immobilization applications [13]. ZnO behaves as network modifier at low concentrations and as former at higher concentrations. The addition of ZnO improves UV optical transparency, enhances the nonlinear optical features, and increases the thermal stability of the glasses [14, 15]. The large polarizability and weak field strength of Bi^{3+} ions in Bi_2O_3 make the element act as glass modifier at low concentrations (~ < 10 mol%) and as glass former at high concentrations (~ > 10 mol%) [15, 16]. Trivalent erbium (Er^{3+}) ion is an efficient rare-earth (RE) ion which can be used in optical amplifiers, due to the prominent $^4I_{13/2} \rightarrow {}^4I_{15/2}$ [near-infrared (NIR)] and $^4I_{11/2} \rightarrow {}^4I_{13/2}$ [mid-infrared (MIR)] transitions at 1.5 µm and 2.7 µm wavelengths, respectively, usually, under 808-nm or 980-nm laser diode pumping [15, 17, 18]. Moreover, Er^{3+} ions emit $^2H_{11/2}/{}^4S_{3/2} \rightarrow {}^4I_{15/2}$ (green light) and $^4F_{9/2} \rightarrow {}^4I_{15/2}$ (red light) upconversion transitions when excited upon 800-nm or 980-nm laser diodes, which is useful in different optoelectronic applications [18, 19].

Here, we have evaluated the shielding capabilities of the Pb-free B_2O_3–ZnO–Bi_2O_3–Er_2O_3 transparent glasses against γ-rays and neutron beam using XCOM. The geometric progression (G-P) fitting approach was employed to determine the MAC, Z_{eff}, N_e, HVL, MFP, and exposure buildup factor (EBF) values within 0.015–15 MeV photon energies. The fast neutron removal cross-section values were also evaluated for the selected glasses. A good agreement within the MAC values was observed when obtained from XCOM, and MCNP5 and Geant4 simulation codes.

2 Materials and methods

The densities of the $(99.5-x)$ $(4ZnO–3B_2O_3) - xBi_2O_3$–0.5 Er_2O_3 ($x=0$, 5, 10, 20, 30, 40, and 60 mol%) glass systems were adopted from Ref. [15]. The seven glasses were denoted as 'S1', 'S2', 'S3', 'S4', 'S5', 'S6', and 'S7' for convenience. Table 1 presents each chemical composition (in mol%) along with their calculated elemental composition (in wt%) values. The samples were fabricated by the standard melt-quenching technique at 800–1200 °C for 45 min. following the particular glass composition. Using the buoyancy principle of Archimedes' law, the densities of the samples were measured, using water as an immersion liquid.

To evaluate practically the radiation shielding performance of different glass or other material systems, occasionally, it is hard to find an appropriate experimental setup due to unavailability of the costly experimental equipment. In these situations, the Monte Carlo simulations are the alternative and definitive method for the accurate measurement of radiation interactions with the selected materials. The XCOM and simulation approaches such as MCNP5 and Geant4 are easy to use and time-saving, to carry out the measurements in a personal computing environment.

Table 1 Chemical composition (mol%) and elements (wt%) present in the selected glasses, including their density [15]

Glass code	Glass compositions (mol%)				Elemental composition (wt%)					Density (g/cm^3)
	B_2O_3	ZnO	Bi_2O_3	Er_2O_3	B	Zn	Bi	Er	O	
S1	42.64	56.86	0	0.5	11.84	47.74	0.0	2.15	38.27	3.651
S2	40.50	54.00	5	0.5	8.99	36.27	21.47	1.72	31.55	4.274
S3	38.36	51.14	10	0.5	7.10	28.62	35.77	1.43	27.08	4.823
S4	34.07	45.43	20	0.5	4.73	19.07	53.65	1.07	21.48	5.869
S5	29.79	39.71	30	0.5	3.31	13.33	64.38	0.86	18.12	6.606
S6	25.50	34.00	40	0.5	2.36	9.51	71.53	0.72	15.88	7.182
S7	16.93	22.57	60	0.5	1.17	4.73	80.47	0.53	13.10	8.111

2.1 *XCOM*

XCOM software program is a database, which is easy to use, can be used to quantify the MAC (μ/ρ) values for elements, compounds, and mixtures ($Z \leq 100$), within the 1 keV–100 GeV energy range [20]. In glasses, each sample can be described by its elemental fractions following the chemical composition (see Table 1). The XCOM program is built on the postulation that the contribution of each element of materials to the 'μ/ρ' is an additive. The computed MAC values for all the samples through the XCOM program were compared with the MAC values simulated by MCNP5 and Geant4 codes to verify the validity of the input file.

2.2 *MCNP5 simulation code*

The Los Alamos National Laboratory (LANL), USA developed the Monte Carlo N Particle (MCNP5) general-purpose code. MCNP5 is a user-friendly model that can be utilized for studying interactions of X-rays, γ-rays and neutrons with materials for radiation shielding applications as well as to evaluate eigenvalues for critical systems. The MCNP5 simulation is a three-dimensional geometric cell using large nuclear pointwise cross-section library data utilizing physics models for different particle types [21]. Gamma-rays were set as a point isotropic source for various photon energies within 0.015–15 MeV range. The absorbed dose was analyzed using average flux tally F4 in the detection area and the yield is given as particles/cm^2. The number of starting particles used during the simulation was 10^8. The Intel® Core™ i7–6700 CPU 3.40 GHz computer hardware was used for MCNP5 computations. The uncertainties in the derived simulated results were less than 0.1% approximately. Figure 1 represents the schematic geometry used in the present work.

2.3 *Geant4 simulation code*

To analyze the interaction and transit of particles through matter, the European Organization for Nuclear Research (CERN), Switzerland and High Energy Accelerator Research Organization (KEK), Japan developed Geometry and Tracking (Geant4)

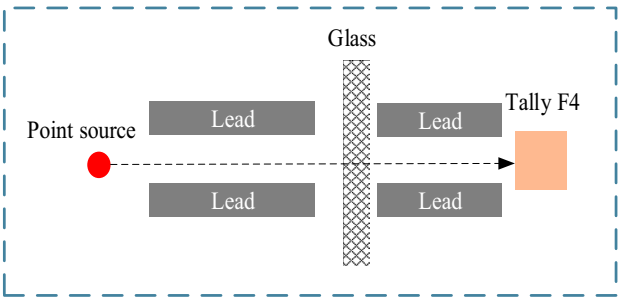

Fig. 1 Simulation setup for MCNP5 code

Monte Carlo simulation toolkit with a collaboration of physicists and software engineers around worldwide [22]. Nowadays, the Geant4 code is widely used in the simulation of experiments in nuclear physics, high-energy physics, medical physics, accelerator design, and space physics. Geant4 contains a broad range of physical models such as photoelectric effect (PE), Compton scattering (CS) and Rayleigh scattering, pair production (PP) and absorption which describes the interactions of particles with the material within the range of 250 eV–TeV, depending on the applications. The accomplishment of the Geant4 toolkit in object-oriented design (in C++ programming language) allows it to be easily extended to achieve the provisions of the user [22]. In this work, the Geant4 model reference data for electromagnetic processes were obtained from the National Institute of Standards and Technology (NIST). The setup for Geant4 simulation includes monoenergetic photons that impact on the sample, at different photon energies, similarly as in MCNP5. Following the Beer–Lambert's law, the MAC values of the samples were analyzed. Beer–Lambert's law considers the incident and attenuated intensity of photons, linear attenuation coefficients, and sample thickness.

2.4 *Theory and assessment of shielding parameters*

2.4.1 Mass attenuation coefficient (MAC)

The matter–photon interaction takes place by various processes, namely, PE effect, CS and PP. A monoenergetic

photon beam gets attenuated due to absorption when transited through a material with initial intensity 'I_0'. The law followed is Beer–Lambert's law, which is given as [23]:

$$I = I_0 e^{-\mu x}, \tag{1}$$

here, the transmitted photon intensity through the matter is given as 'I', the linear attenuation coefficient is expressed as 'μ' and 'x' is the material thickness. Equation (1) can also be expressed as:

$$\mu = \frac{-\ln\left(\frac{I}{I_0}\right)}{x}. \tag{2}$$

The MAC estimates the possibility of photon–matter interaction per unit thickness, and is evaluated using the XCOM program by employing the mixture rule [20]:

$$(\mu/\rho)_{\text{glass}} = \sum_i w_i (\mu/\rho)_i, \tag{3}$$

here, the weight fraction is denoted as 'w_i' and MAC of the 'i'th constituent element is given as '$(\mu/\rho)_i$'.

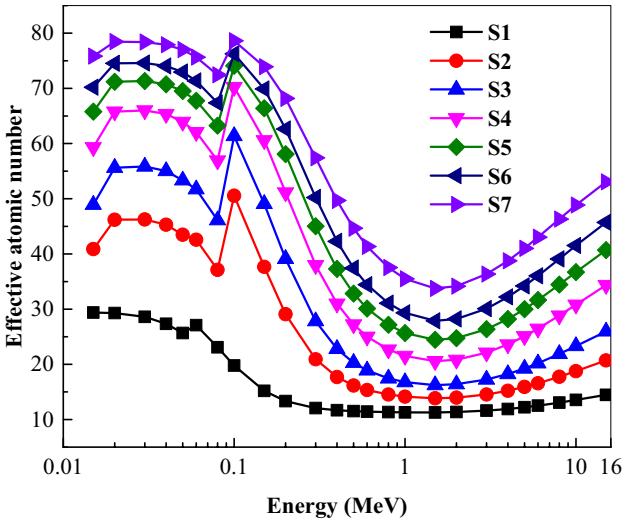

Fig. 3 Variation of effective atomic number with photon energy for S1 → S7 glasses

2.4.2 *Effective atomic number (Z_{eff}) and electron density (N_e)*

The Z_{eff} of a compound cannot be defined by a single number. It is weighed depending upon photon interaction with matter at different energy ranges. The 'Z_{eff}' of the

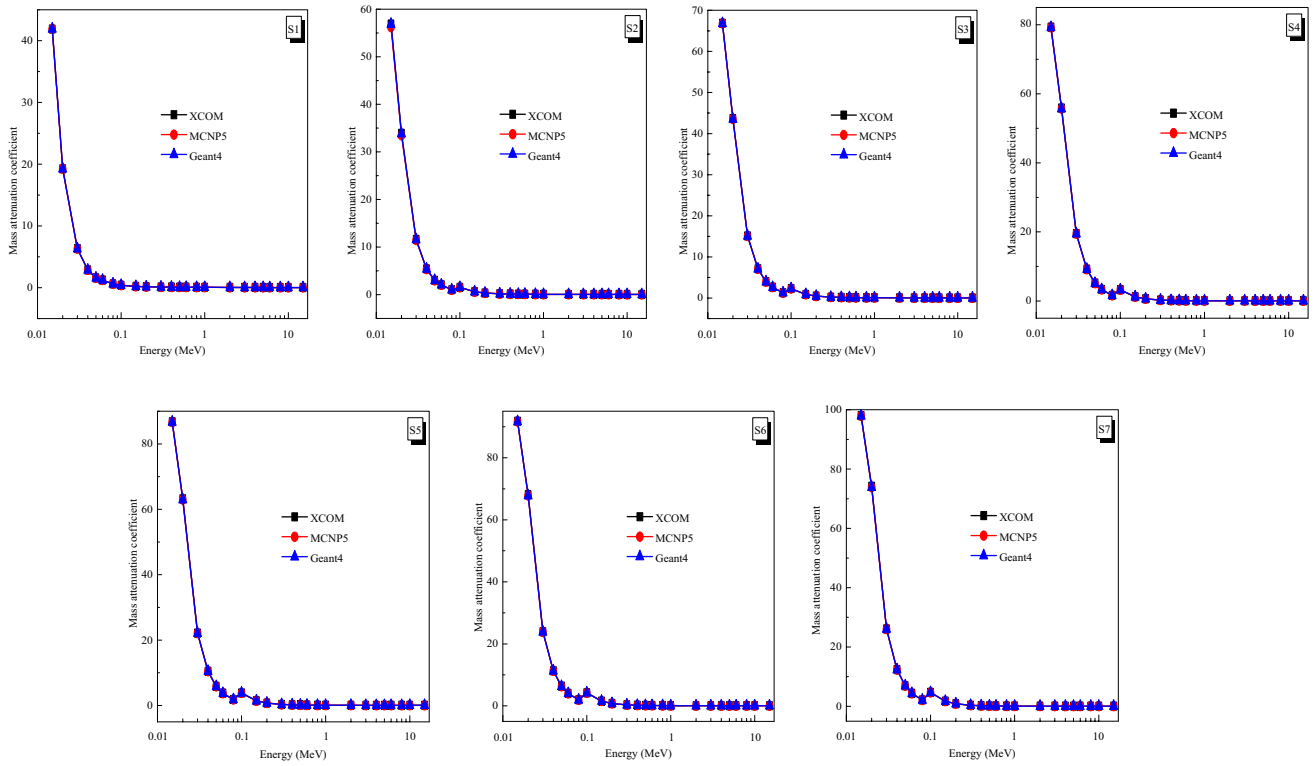

Fig. 2 Comparison of the XCOM, MCNP5, and Geant4 calculated values of mass attenuation coefficients (cm^2/g) versus photon energy for the studied samples

Er_2O_3-doped glasses is computed following the equation [24]:

$$Z_{\text{eff}} = \frac{\sum_i f_i A_i \left(\frac{\mu}{\rho}\right)_i}{\sum_j f_j \frac{A_j}{Z_j} \left(\frac{\mu}{\rho}\right)_j}, \tag{4}$$

here, 'f_i' is the fractional abundance, 'A_i' is the atomic weight, and 'Z_i' is the atomic number of the ith element.

The aggregate electrons per unit mass in the experimenting material is defined as N_e. Higher the N_e value, larger the probability of photon interaction.

The 'N_e' can be derived by the expression [24]:

$$N_e = N_A \frac{nZ_{\text{eff}}}{\sum_i n_i A_i} = N_A \frac{Z_{\text{eff}}}{A}, \tag{5}$$

where mean atomic mass is represented as 'A' and 'N_A' is the Avogadro constant.

2.4.3 Half-value layer (HVL) and mean free path (MFP)

HVL is identified when 50% of the incident radiation is attenuated at a particular thickness of the shielding specimen. HVL is determined using the relation given below [25]:

$$\text{HVL} = \frac{\ln(2)}{\mu} = \frac{0.693}{\mu}. \tag{6}$$

A median distance traveled by γ-rays between subsequent collisions in the matter is defined as MFP. The MFP (in cm) is indirectly proportional to linear attenuation coefficient [25]:

$$\text{MFP} = \frac{1}{\mu}, \tag{7}$$

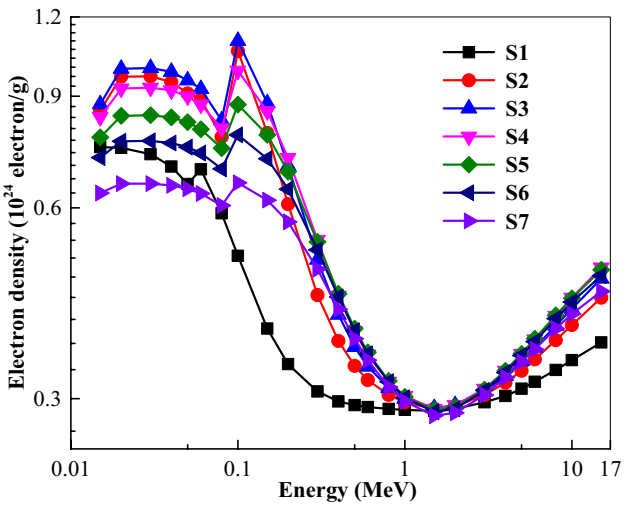

Fig. 4 Variation of electron density with photon energy for S1 → S7 glasses

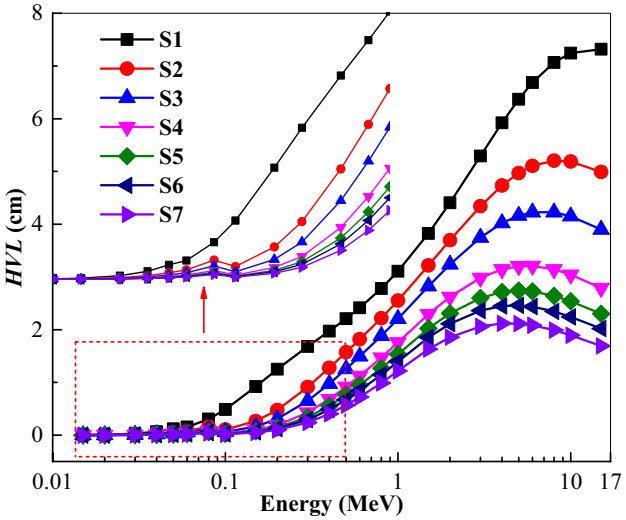

Fig. 5 Variation of half-value layer (HVL) with photon energy for S1 → S7 glasses

here, linear attenuation coefficient is denoted as 'μ'.

Both HVL and MFP are important parameters to examine a material's radiation shielding effectiveness.

2.4.4 Exposure buildup factor (EBF)

The Beer–Lambert's law (i.e., Eq. 1) is applicable when the incident beam is monoenergetic, narrow and interaction takes place with a thin absorbing medium for attenuation. If these conditions do not hold good, then the law can be modified as ($I = BI_0e^{-\mu x}$), where 'B' is buildup factor. The 'B' is a factor describing the interaction and

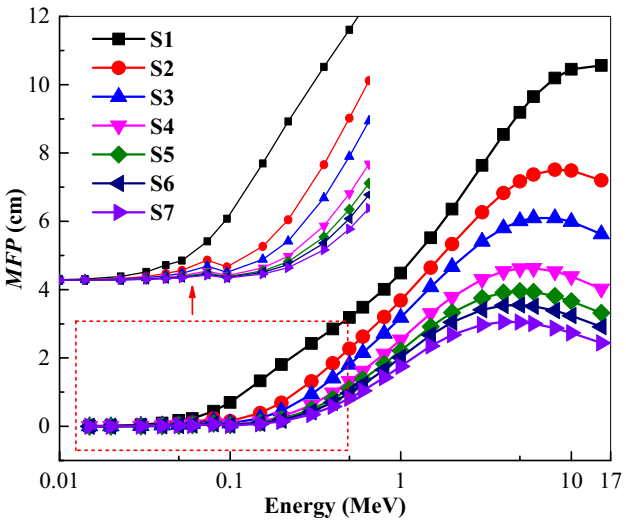

Fig. 6 Variation of mean free path (MFP) with photon energy for S1 → S7 glasses

distribution of photon flux in matter. It majorly relies on the energy of the incident radiation and the characteristics of the material. In the present work, logarithmic interpolation method through G-P fitting parameters using equivalent atomic numbers (Z_{eq}) of the sample was used to compute EBF.

The EBF calculation method can be stated as [26, 27]:

1. Calculating the Z_{eq} values for the selected samples.
2. Evaluation of G-P fitting parameters.
3. Derivation of EBF values.

The related formulae for the EBF calculations are described in the relevant section.

2.4.5 *Macroscopic effective removal cross-sections for fast neutrons (Σ_R)*

The macroscopic effective removal cross-section for fast neutrons ($\sum_R$) is a measure of the probability of neutron beams engaged in definitive reaction per unit length during transit via a shielding medium. The $\sum_R$ is calculated using the below equation [1, 28]:

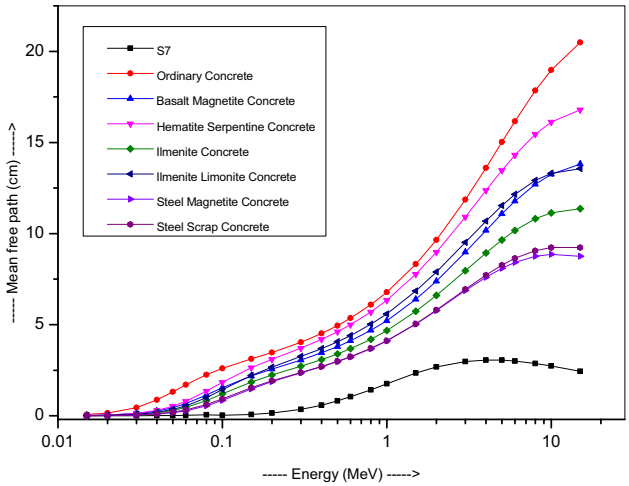

Fig. 8 Comparison of MFP of the sample S7 with some standard shielding concretes

$$\sum R = \sum_i \rho_i \left(\sum R/\rho \right)_i . \tag{8}$$

Here, '$\sum_{R/\rho}$' (cm^2/g) is the mass removal cross-section of the ith constituent and 'ρ_i' (g/cm^3) represents partial density.

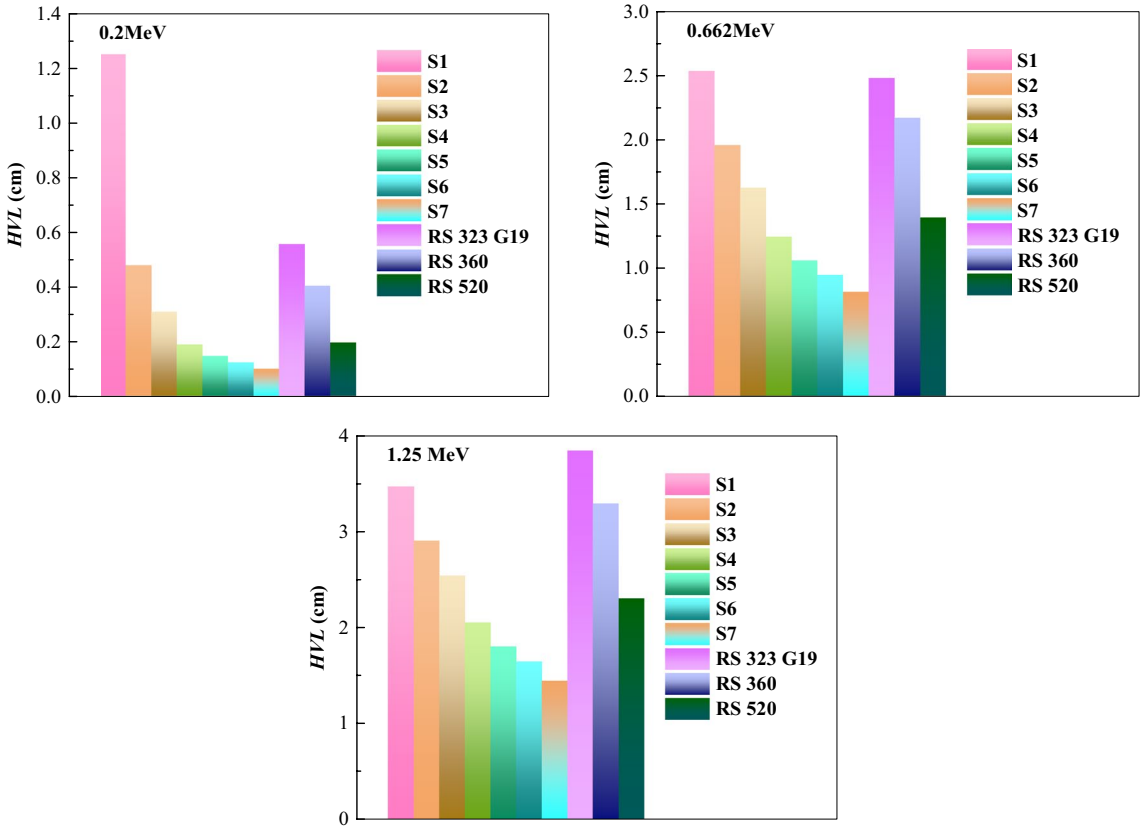

Fig. 7 Comparison of the S1 → S7 samples HVL values with some gamma-ray shielding glasses

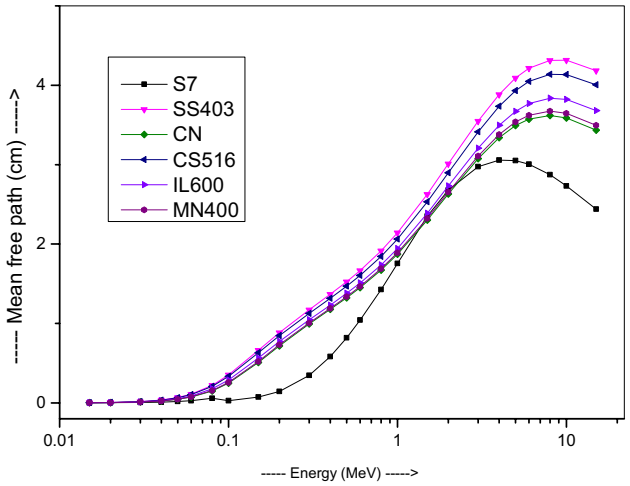

Fig. 9 Comparison of MFP of the sample S7 with some standard alloys

3 Results and discussion

Figure 2 represents the comparison of MAC values of S1−S7 glasses calculated using XCOM, MCNP5 and Geant4 codes within 0.015–15 MeV photon energy. The figure shows an increase in MAC values with an increment in Bi_2O_3 content and decreases with increase in photon energy. This specifies that photon interaction is prominent at higher Bi_2O_3 concentrations and low photon energy. From Fig. 2, it is understood that there is very good accord among MAC values computed through XCOM, MCNP5 and Geant4 codes. Further, the MAC values decreased sharply at low-energy regions due to PE effect (directly depends upon photon energy, $E^{-3.5}$) as shown in Fig. 2. It can also be noticed that MAC values decrease moderately in medium energy region due to CS (depends upon E^{-1}). An increase in MAC values at high-energy region occurs due to PP process. The observed discontinuities or small peaks in the graph are in the vicinity of *M*, *L* and *K* absorption edges of 'Bi' element existing in the sample [29]. The results show that S7 sample owes the highest MAC values, which makes it a better radiation absorber than other samples.

The variation of Z_{eff} values in the energy range of 0.015–15 MeV for all Er_2O_3-doped glasses is shown in Fig. 3. All the samples containing Bi_2O_3 (i.e., S2−S7) showed an equivalent trend with an incident photon. The cross-section for PE absorption is Z^{4-5}, Compton scattering is Z and for pair production, it is Z^2 [1]. Thus, the

Table 2 Equivalent atomic number (Z_{eq}) for samples S1−S7

Energy (MeV)	Equivalent atomic number (Z_{eq})						
	S1	S2	S3	S4	S5	S6	S7
0.015	22.63	25.7	27.8	56.65	59.4	61.23	63.51
0.02	23.02	28.33	32.26	36.75	39.19	40.75	73.77
0.03	23.47	29.07	33.01	37.11	39.3	40.69	42.52
0.04	23.72	29.72	33.56	37.51	39.6	40.91	42.67
0.05	23.89	30.19	33.98	37.85	39.87	41.14	42.89
0.06	25.85	31.76	35.09	38.59	40.45	41.61	43.36
0.08	26.25	32.31	35.59	39.04	40.87	42.03	43.8
0.1	26.55	46.66	54.57	62.93	67.73	70.74	74.27
0.15	27.0	48.3	56.26	64.5	69.12	71.9	75.31
0.2	27.27	49.3	57.29	65.44	69.84	72.52	75.83
0.3	27.62	50.57	58.51	66.45	70.62	73.21	76.36
0.4	27.84	51.27	59.19	66.98	71.04	73.63	76.63
0.5	27.98	51.73	59.63	67.3	71.31	73.9	76.78
0.6	28.08	52.02	59.92	67.5	71.5	74.09	76.89
0.8	28.18	52.36	60.24	67.72	71.7	74.28	76.98
1.0	28.21	52.49	60.37	67.81	71.78	74.36	77.02
1.5	25.2	50.57	58.84	66.81	70.95	73.75	76.6
2.0	21.31	44.34	54.15	63.87	68.54	71.67	75.34
3.0	19.69	35.86	45.86	57.14	63.36	67.28	72.12
4.0	19.24	32.88	41.93	53.15	59.81	64.2	69.67
5.0	19.04	31.47	40.0	50.91	57.66	62.27	68.14
6.0	18.91	30.62	38.95	49.63	56.4	61.09	67.14
8.0	18.78	29.7	37.8	48.17	54.95	59.69	65.91
10.0	18.72	29.2	37.21	47.37	54.13	58.88	65.19
15.0	18.66	28.87	36.79	46.67	53.32	58.03	64.36

Table 3 G-P fitting parameters for sample S1

Energy (MeV)	G-P fitting parameters				
	b	*c*	*a*	x_k	*d*
0.015	1.006	1.05	− 0.25	6.36	0.2342
0.02	1.014	0.275	0.416	11.16	− 0.3691
0.03	1.039	0.373	0.204	22.38	− 0.2393
0.04	1.083	0.346	0.243	12.5	− 0.1247
0.05	1.14	0.379	0.226	14.05	− 0.1295
0.06	1.152	0.406	0.208	14.17	− 0.1141
0.08	1.26	0.468	0.181	14.43	− 0.0985
0.1	1.37	0.547	0.148	14.07	− 0.0816
0.15	1.611	0.72	0.086	14.08	− 0.0503
0.2	1.776	0.878	0.042	13.4	− 0.0347
0.3	1.913	1.055	− 0.001	12.22	− 0.0191
0.4	1.939	1.154	− 0.021	11.18	− 0.0138
0.5	1.928	1.206	− 0.032	9.4	− 0.0096
0.6	1.906	1.225	− 0.036	8.43	− 0.0092
0.8	1.862	1.228	− 0.037	7.26	− 0.0116
1.0	1.822	1.216	− 0.038	10.49	− 0.005
1.5	1.756	1.199	− 0.04	15.88	0.0112
2.0	1.731	1.142	− 0.028	15.24	0.0046
3.0	1.646	1.063	− 0.009	12.63	− 0.008
4.0	1.578	1.004	0.009	11.68	− 0.0179
5.0	1.508	0.986	0.013	13.4	− 0.0201
6.0	1.463	0.959	0.023	13.44	− 0.0283
8.0	1.382	0.932	0.033	13.45	− 0.0377
10.0	1.317	0.925	0.038	13.5	− 0.0423
15.0	1.227	0.894	0.055	13.61	− 0.0583

Table 4 G-P fitting parameters for sample S2

Energy (MeV)	G-P fitting parameters				
	B	*c*	*a*	x_k	*d*
0.015	1.004	1.518	− 0.528	5.66	0.3425
0.02	1.01	0.109	0.733	10.91	− 0.9664
0.03	1.037	0.364	0.204	12.16	− 0.0527
0.04	1.226	0.331	0.227	15.49	− 0.0959
0.05	1.278	0.319	0.192	13.29	− 0.1202
0.06	1.088	0.411	0.209	13.72	− 0.1142
0.08	1.153	0.415	0.216	13.74	− 0.131
0.1	1.113	0.286	0.32	13.07	− 0.2009
0.15	1.131	0.605	0.111	13.71	− 0.0509
0.2	1.237	0.546	0.148	14.61	− 0.0775
0.3	1.387	0.641	0.116	14.34	− 0.071
0.4	1.484	0.749	0.077	14.23	− 0.0485
0.5	1.556	0.833	0.054	13.89	− 0.0401
0.6	1.6	0.891	0.037	13.95	− 0.0323
0.8	1.627	0.95	0.021	13.9	− 0.0234
1.0	1.644	0.992	0.009	13.66	− 0.0178
1.5	1.612	1.077	− 0.013	12.51	− 0.0067
2.0	1.609	1.09	− 0.011	12.52	− 0.0139
3.0	1.588	1.049	0.002	12.65	− 0.0251
4.0	1.533	1.016	0.014	13.06	− 0.0341
5.0	1.489	0.993	0.022	13.34	− 0.0399
6.0	1.441	0.981	0.027	13.32	− 0.0444
8.0	1.362	0.956	0.04	13.54	− 0.0569
10.0	1.293	0.962	0.042	13.91	− 0.0582
15.0	1.191	0.969	0.052	14.48	− 0.0638

Z_{eff} values evaluated for S1−S7 samples increase with the Bi_2O_3 content increment since the effective atomic cross-section of Bi_2O_3 is higher than that of ZnO. Figure 3 shows a decrease in the Z_{eff} values at low-energy region and a sharp rise for the same in S2−S7 samples at the photon energy about 0.1 MeV, where PE effects are dominant, which could be due to 'Bi' element absorption edge (*K*-edge) at 0.09052 MeV. Usually, the *K* absorption edge of 'Zn' element lies at 9.659 keV. Thereafter, Z_{eff} values are sharply decreased within the photon energy range of 0.1−1.0 MeV, where CS gradually becomes an efficient interaction. Then on, from 1.0 to 15 MeV, PP interaction is prevalent and Z_{eff} values see a moderate increase [30]. Generally, a high value of Z_{eff} in materials makes it a promising shield against radiation. Here, sample S7 possesses the highest value of Z_{eff}, suggesting it as a better radiation absorber.

The comparison in the N_e values for all samples is shown in Fig. 4, for 0.015−15 MeV energy of photons. From Fig. 4, one can see that S1 sample shows the lowest values for N_e except in the energy region of 0.015−0.1 MeV, where it shows slightly higher values concerning S7 sample. Further, for S2−S7 samples, with Bi_2O_3 content, the N_e values decrease and the S7 sample possesses the lowest N_e values. N_e and Z_{eff} values observed a similar trend because both are directly proportional to each other.

The HVL values evaluated for S1−S7 samples within 0.015−15 MeV photon energy are depicted in Fig. 5. Similarly, the variation of the MFP values with different incident photon energies (0.015−15 MeV range) are shown in Fig. 6 for all the selected glasses, which shows a similar trend as HVL values. We know that lower the HVL and MFP values of a material are, better the gamma radiation shield. Figures 5 and 6 exhibit small values of HVL and MFP in S1−S7 samples at lower energy region, $E \leq 0.1$ MeV. Further, both HVL and MFP increase up to 5−10 MeV photon energy range depending on the added Bi_2O_3 content in the samples and then indicates a slight decrement with further increased photon energy. The variations of HVL and MFP values in S1−S7 glass samples with photon energy are due to the different photon interactions at different energy, hence in agreement with MAC values. This also suggests that the selected glasses can attenuate low-energy photons very well at lower thickness than those of higher energy. From Figs. 5 and 6, it is reviewed that both HVL and MFP values are the lowest

Table 5 G-P fitting parameters for sample S3

Energy (MeV)	G-P fitting parameters				
	b	*c*	*a*	x_k	*d*
0.015	1.002	1.857	− 0.404	9.0	0.2908
0.02	1.01	0.182	0.616	11.81	− 0.7983
0.03	1.93	0.615	0.172	20.49	− 0.1411
0.04	2.146	0.336	0.164	20.7	− 0.0946
0.05	1.889	0.218	0.042	14.45	− 0.0598
0.06	1.066	0.463	0.178	13.91	− 0.0915
0.08	1.12	0.388	0.238	13.53	− 0.1502
0.1	1.715	0.22	0.04	15.19	− 0.0301
0.15	1.42	0.1	0.604	14.42	− 0.161
0.2	1.092	0.531	0.139	13.66	− 0.0663
0.3	1.206	0.48	0.182	14.45	− 0.0987
0.4	1.316	0.632	0.115	14.28	− 0.0665
0.5	1.415	0.725	0.084	14.02	− 0.0496
0.6	1.478	0.805	0.059	13.94	− 0.0395
0.8	1.528	0.871	0.04	13.84	− 0.0303
1.0	1.563	0.939	0.021	13.68	− 0.0221
1.5	1.585	0.995	0.007	13.47	− 0.0158
2.0	1.571	1.061	− 0.008	12.7	− 0.0113
3.0	1.536	1.05	0.004	13.02	− 0.0321
4.0	1.509	1.003	0.023	13.32	− 0.0501
5.0	1.518	0.949	0.043	13.58	− 0.066
6.0	1.499	0.92	0.055	13.7	− 0.0768
8.0	1.455	0.92	0.061	13.94	− 0.0793
10.0	1.438	0.944	0.059	14.08	− 0.0767
15.0	1.432	1.041	0.047	14.15	− 0.0678

Table 6 G-P fitting parameters for sample S4

Energy (MeV)	G-P fitting parameters				
	b	*c*	*a*	x_k	*d*
0.015	1.002	0.352	0.27	15.02	− 0.1812
0.02	1.01	0.278	0.435	13.06	− 0.477
0.03	2.752	0.846	0.142	28.16	− 0.2224
0.04	2.986	0.34	0.108	25.46	− 0.0934
0.05	2.444	0.127	− 0.094	15.51	− 0.0048
0.06	1.044	0.512	0.149	14.1	− 0.0699
0.08	1.089	0.362	0.259	13.33	− 0.1687
0.1	1.666	0.242	− 0.022	19.13	0.0621
0.15	1.179	0.18	0.422	13.24	− 0.2537
0.2	1.159	0.368	0.249	13.99	− 0.1355
0.3	1.218	0.556	0.143	14.35	− 0.0773
0.4	1.299	0.643	0.108	14.03	− 0.0582
0.5	1.363	0.725	0.082	14.11	− 0.0467
0.6	1.409	0.783	0.064	13.86	− 0.0393
0.8	1.467	0.845	0.045	13.68	− 0.0298
1.0	1.497	0.901	0.03	13.53	− 0.0243
1.5	1.504	0.991	0.006	13.07	− 0.0136
2.0	1.497	1.017	0.007	13.0	− 0.0234
3.0	1.534	1.053	− 0.002	12.94	− 0.0191
4.0	1.469	1.033	0.014	13.18	− 0.0428
5.0	1.473	0.978	0.038	13.67	− 0.0653
6.0	1.487	0.923	0.062	13.89	− 0.087
8.0	1.482	0.936	0.064	14.21	− 0.0851
10.0	1.509	0.971	0.063	14.06	− 0.0853
15.0	1.571	1.135	0.037	13.89	− 0.0663

for S7 sample (60 mol% Bi_2O_3 inclusion) and are largest for S1 (without any Bi_2O_3 content addition). This implies that sample S7 is the promising gamma-ray shielding glass compared with remaining samples selected for this study as density (μ/ρ), and Z_{eff} values for glass S7 are highest while S1 sample possesses the least values for these parameters (i.e., density, MAC, and Z_{eff}). Thus, for glass systems, the chemical composition can affect the HVL and MFP values, so by tuning the compositions to an optimum level in terms of density and Z_{eff}, one can achieve the required radiation shielding effectiveness for the glasses [31].

Figure 7 compares the values of HVL in S1−S7 samples with some commercially available SCOTT company radiation shielding glasses such as RS 323 G19, RS 360, and RS 520 at photon energies of 0.2 MeV, 0.662 MeV, and 1.25 MeV. From Fig. 7, one can notice that at all 0.2 MeV, 0.662 MeV, and 1.25 MeV gamma-ray energies, HVL values of S4−S7 samples are lower than that of all the SCOTT glasses, while the S1 glass possesses relatively higher HVL value compared to the RS 323 G19, RS 360, and RS 520 glasses at 0.2 MeV and 0.662 MeV photon energies, respectively. Moreover, at 0.2 MeV photon energy, HVL values of the S2 and S3 glasses lie in between the RS 323 G19 and RS 360, RS 360 and RS 520 glasses, respectively. At 0.662 MeV, the HVL values of S2 and S3 glasses lie in between the RS 360 and RS 520 sample values. Further, at 1.25 MeV gamma energy, S2−S7 samples showed similar HVL trend as was observed in the samples at 0.662 MeV energy. But S1 sample exhibited higher HVL values than RS 360 and RS 520 glasses and lower than RS 323 and G19 glasses. The high atomic number elements like, Er, and Bi in the studied glasses increase matter–photon interaction, leading to an increase in radiation attenuation performance. From Fig. 7, one can observe that at all the compared energies, S7 sample possesses the lowest values of HVL than the selected SCOTT shielding glasses, confirming the fact that the S7 glass radiation shielding effectiveness is better than that of these commercial glasses.

To implement for practical shielding applications at nuclear reactor sites and medical diagnostics laboratories, it is primary to collate the MFP values of the Er_2O_3-doped glasses with some different shielding concretes and alloys. In this regard, MFP values of seven types of standard shielding concrete [32] and five types of shielding alloys

Table 7 G-P fitting parameters for sample S5

Energy (MeV)	G-P fitting parameters				
	b	*c*	*a*	x_k	*d*
0.015	1.002	0.466	0.2	17.55	− 0.103
0.02	1.011	0.325	0.346	13.68	− 0.3182
0.03	3.155	0.959	0.127	31.91	− 0.2623
0.04	3.394	0.343	0.08	27.78	− 0.0928
0.05	2.713	0.082	− 0.16	16.02	0.0218
0.06	1.034	0.536	0.135	14.19	− 0.0592
0.08	1.074	0.349	0.269	13.23	− 0.1779
0.1	1.665	0.499	0.056	18.23	− 0.0123
0.15	1.218	0.166	0.378	14.41	− 0.1624
0.2	1.157	0.307	0.297	13.83	− 0.1645
0.3	1.19	0.522	0.154	13.94	− 0.0764
0.4	1.26	0.624	0.114	14.13	− 0.0598
0.5	1.321	0.698	0.089	14.16	− 0.0488
0.6	1.365	0.758	0.07	14.0	− 0.0408
0.8	1.427	0.816	0.053	13.65	− 0.0325
1.0	1.462	0.867	0.039	13.54	− 0.0269
1.5	1.476	0.966	0.012	13.17	− 0.0155
2.0	1.467	1.001	0.01	13.12	− 0.0236
3.0	1.452	1.039	0.009	13.3	− 0.035
4.0	1.444	1.045	0.012	13.21	− 0.0412
5.0	1.432	1.02	0.025	13.42	− 0.0556
6.0	1.468	0.963	0.048	13.74	− 0.0759
8.0	1.47	0.94	0.062	14.02	− 0.0862
10.0	1.484	0.979	0.06	14.08	− 0.0843
15.0	1.534	1.114	0.04	13.91	− 0.0686

Table 8 G-P fitting parameters for sample S6

Energy (MeV)	G-P fitting parameters				
	b	*c*	*a*	x_k	*d*
0.015	1.001	0.55	0.147	19.87	− 0.0539
0.02	1.011	0.354	0.292	14.06	− 0.2219
0.03	3.399	1.027	0.118	34.19	− 0.2864
0.04	3.64	0.344	0.063	29.17	− 0.0924
0.05	2.874	0.056	− 0.2	16.33	0.0377
0.06	1.027	0.551	0.126	14.24	− 0.0527
0.08	1.068	0.34	0.277	13.18	− 0.1832
0.1	1.709	0.693	0.103	17.17	− 0.0687
0.15	1.241	0.158	0.353	15.08	− 0.1102
0.2	1.156	0.272	0.325	13.73	− 0.1813
0.3	1.174	0.503	0.16	13.7	− 0.0759
0.4	1.237	0.613	0.118	14.18	− 0.0608
0.5	1.295	0.682	0.094	14.19	− 0.0501
0.6	1.338	0.743	0.074	14.08	− 0.0414
0.8	1.401	0.799	0.057	13.69	− 0.0335
1.0	1.437	0.85	0.043	13.68	− 0.0276
1.5	1.458	0.949	0.016	13.23	− 0.0167
2.0	1.448	0.992	0.012	13.19	− 0.0235
3.0	1.426	1.035	0.011	13.32	− 0.0364
4.0	1.391	1.036	0.02	13.48	− 0.0509
5.0	1.436	0.981	0.042	13.7	− 0.0698
6.0	1.452	0.956	0.054	13.9	− 0.08
8.0	1.463	0.961	0.059	14.0	− 0.0839
10.0	1.478	1.002	0.056	14.07	− 0.081
15.0	1.508	1.088	0.043	13.93	− 0.0707

[33] were compared with the MFP values of S7 glass within 0.015−15 MeV photon energy and is shown in Figs. 8 and 9, respectively. Apparently, from Figs. 8 and 9, one can see that within the studied gamma-ray energy range, the MFP value of S7 glass is smaller in comparison to these commonly used standard shielding concretes and the selected alloys. Therefore, S7 glass can be a potential γ-ray shielding material.

The ratio of Compton partial mass attenuation coefficient (μ_c) and the total mass attenuation coefficient (μ_T) gives the equivalent atomic number (Z_{eq}). This ratio can be obtained using WinXCom software. The formula used to obtain Z_{eq} is given as [26]:

$$Z_{eq} = \frac{Z1(\log R2 - \log R) + Z2(\log R - \log R1)}{\log R2 - \log R1}, \quad (9)$$

where 'Z_1' is the atomic number of an element having ratio 'R_1' and 'Z_2' is the atomic number of an element having ratio 'R_2'. 'R' be the ratio of the glasses (S1−S7) at photon energy range from 0.015 to 15 MeV. The evaluated values of the 'Z_{eq}' for S1−S7 samples are listed in Table 2.

With the help of values Z_{eq}, the five G-P parameters (*b*, *c*, *a*, x_k, and *d*) were calculated using the following relation [26]:

$$P = \frac{P1(\log Z2 - \log Z_{eq}) + P2(\log Z_{eq} - \log Z1)}{\log Z2 - \log Z1}, \quad (10)$$

where 'P_1' and 'P_2' are G-P fitting parameters corresponding to Z_1 and Z_2, respectively. The values of all these parameters are presented in Tables 3, 4, 5, 6, 7, 8 and 9.

The EBF was calculated using G-P fitting parameters for 25 standard energies at different penetration depths (up to 40 mfp) using the following relations [27]:

$$B(E,x) = \frac{b-1}{K-1}(K^x - 1) \quad \text{for} \quad K \neq 1, \quad (11)$$

$$B(E,x) = 1 + (b-1)x \quad \text{for} \quad K = 1, \quad (12)$$

here, photon dose multiplication factor is represented as a function *K(E, x),* whose relation is given as:

$$K(E,x) = cx^a + d\frac{\tanh(x/X_k - 2) - \tan h(-2)}{1 - \tan h(-2)} \quad \text{for} \quad x \leq 40\,\text{mfp}, \quad (13)$$

Table 9 G-P fitting parameters for sample S7

Energy (MeV)	G-P fitting parameters				
	b	*c*	*a*	x_k	*d*
0.015	1.001	0.652	0.082	22.69	0.0055
0.02	1.002	0.259	0.392	13.14	− 0.317
0.03	3.57	1.144	0.105	34.37	− 0.2894
0.04	3.806	0.425	0.054	30.01	− 0.0948
0.05	3.03	0.093	− 0.165	16.56	0.0142
0.06	1.359	0.497	0.095	12.56	− 0.0513
0.08	1.234	0.263	0.404	13.65	− 0.178
0.1	1.765	0.913	0.149	16.15	− 0.1259
0.15	1.283	0.188	0.326	16.57	− 0.0763
0.2	1.162	0.238	0.35	13.58	− 0.1895
0.3	1.155	0.508	0.154	13.65	− 0.0713
0.4	1.2	0.631	0.107	16.02	− 0.0512
0.5	1.253	0.697	0.086	14.44	− 0.0409
0.6	1.298	0.743	0.07	14.23	− 0.033
0.8	1.358	0.799	0.054	14.23	− 0.0283
1.0	1.394	0.853	0.04	14.69	− 0.0232
1.5	1.429	0.929	0.02	13.26	− 0.0168
2.0	1.427	0.977	0.015	13.26	− 0.024
3.0	1.401	1.03	0.012	13.3	− 0.0363
4.0	1.365	1.038	0.019	13.62	− 0.0487
5.0	1.407	0.986	0.042	13.87	− 0.0683
6.0	1.427	0.95	0.059	14.06	− 0.0831
8.0	1.449	1.001	0.055	14.13	− 0.0773
10.0	1.495	1.084	0.044	13.93	− 0.0712
15.0	1.588	1.271	0.022	13.68	− 0.0558

where '*E*' is the incident photon energy, '*x*' is the distance between source to the detector in the medium, and '*b*' is the buildup factor at 1 mfp.

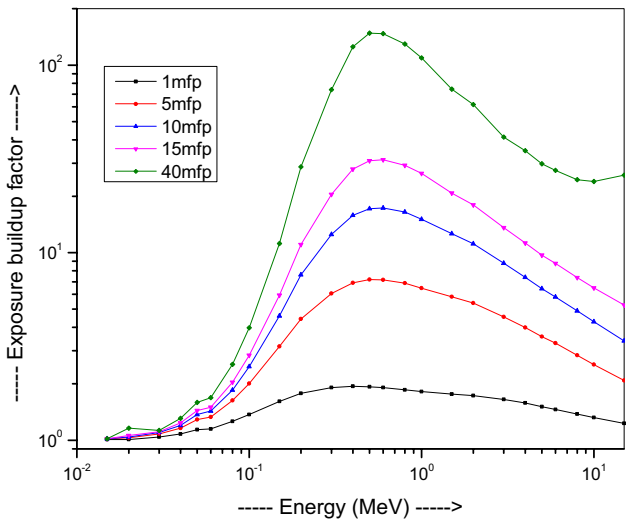

Fig. 10 Variation of EBF with energy for S1 sample at different mean free path

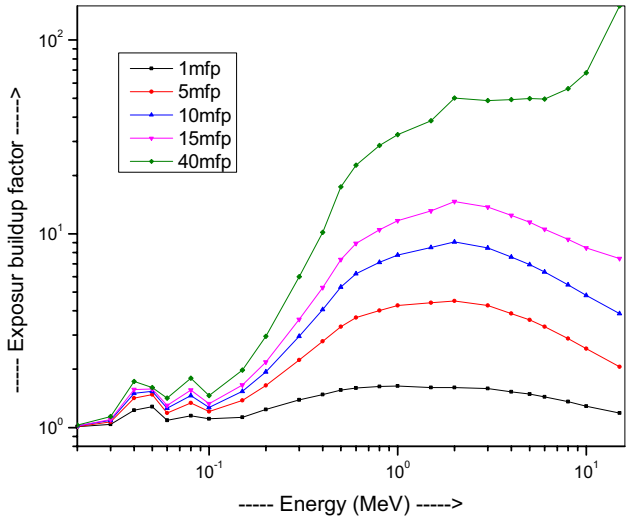

Fig. 11 Variation of EBF with energy for S2 sample at different mean free path

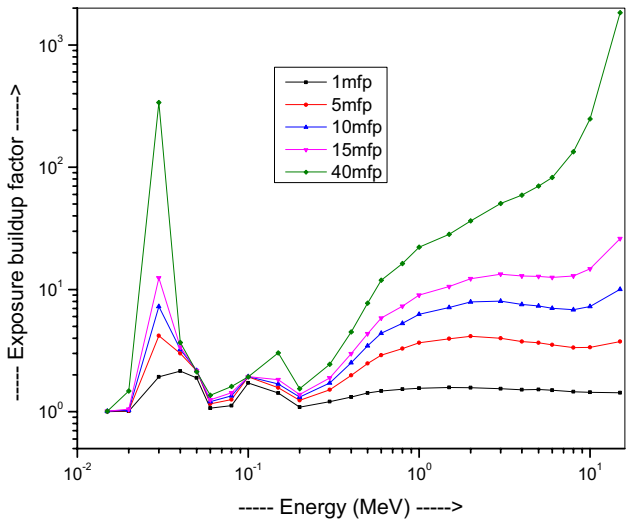

Fig. 12 Variation of EBF with energy for S3 sample at different mean free path

Figures 10, 11, 12, 13, 14, 15 and 16 represent the variation of EBF for S1−S7 glasses, within 0.015–15 MeV photon energy and at different penetration depths changing from 1 to 40 mfp. EBF values increase as penetration depth increases in all the glasses, which in turn increases the scattering processes. One can notice from Figs. 10, 11, 12, 13, 14, 15 and 16 that the values of EBF are very small in the low-energy region, which may be due to the PE effect dominance. Around 1 MeV, the EBF values improve with increment in energy, due to CS, which then degrades the photon energy. As these photons retain for long in the material, degradation of photon energy takes place as a result

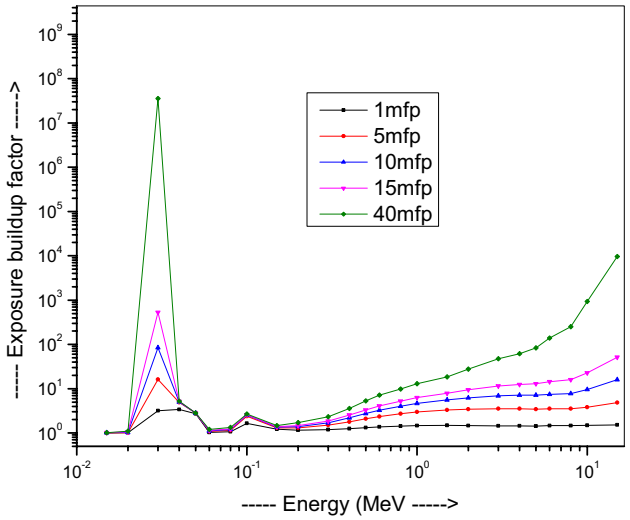

Fig. 13 Variation of EBF with energy for S4 sample at different mean free path

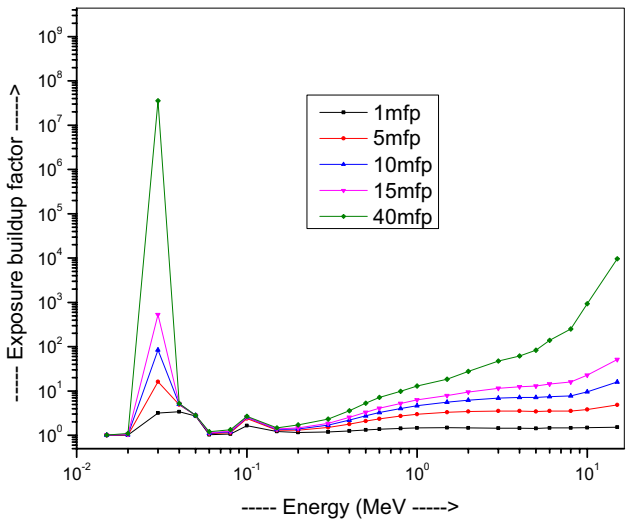

Fig. 14 Variation of EBF with energy for S5 sample at different mean free path

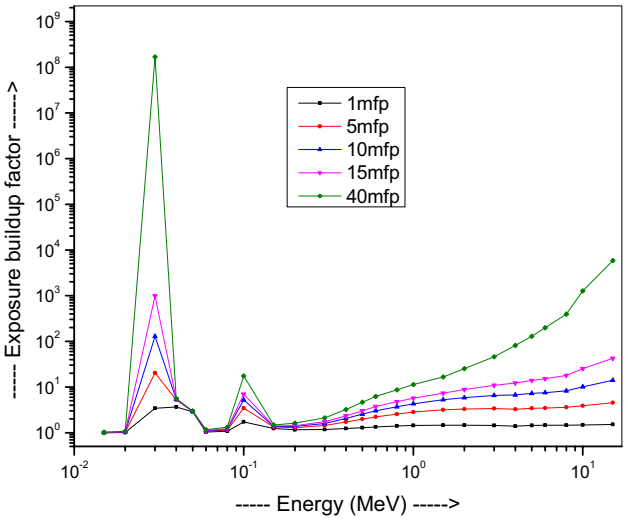

Fig. 15 Variation of EBF with energy for S6 sample at different mean free path

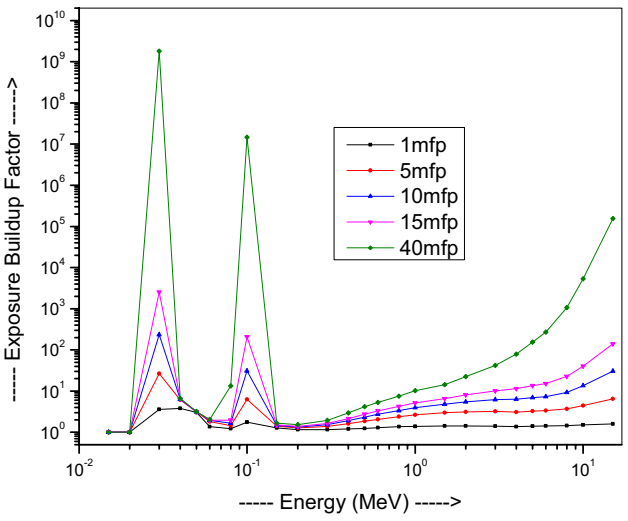

Fig. 16 Variation of EBF with energy for S7 sample at different mean free path

of CS, hence, a higher value of EBF factor. At $E > 1$ MeV, EBF values decrease due to the absorption behavior of the PP process.

The removal cross-section for fast neutrons ($\sum_R$) value for the S1−S7 glasses was computed using Eq. (8) and the results are shown in Fig. 17. It was found that the $\sum_R$ values are varied within the range 0.1142–0.1232 cm^{-1} for S1−S7 glasses. The ($\sum_R$) values slightly increase with the Bi_2O_3 content in S4−S7 samples. From Table 1, one can notice that wt% of Bi element in the samples increases at the cost of B, Zn, and O elements. However, the ($\Sigma_R/_\rho$) value of B and O elements is higher than that of the 'Bi' element. Though the low-Z elements (B, and O) are responsible for better neutron removal, one can expect that a mixture of both low and high Z elements (e.g. Bi) could also achieve similar results in the glasses. The highest value of ($\sum_R$) was found for S7, indicating S7 to be the most effective neutron shield when compared to the other glasses. Further, the ($\sum_R = 0.1232$ cm^{-1}) value of the sample S7 in this work is larger in comparison to ordinary concrete ($\sum_R = 0.094$ cm^{-1}) and hematite–serpentine ($\sum_R = 0.097$ cm^{-1}) [34] including TeO_2–B_2O_3 glass ($\sum_R = 0.12039$ cm^{-1}) [35] and K30W60T10 glass ($\sum_R = 0.12087$ cm^{-1}) [36].

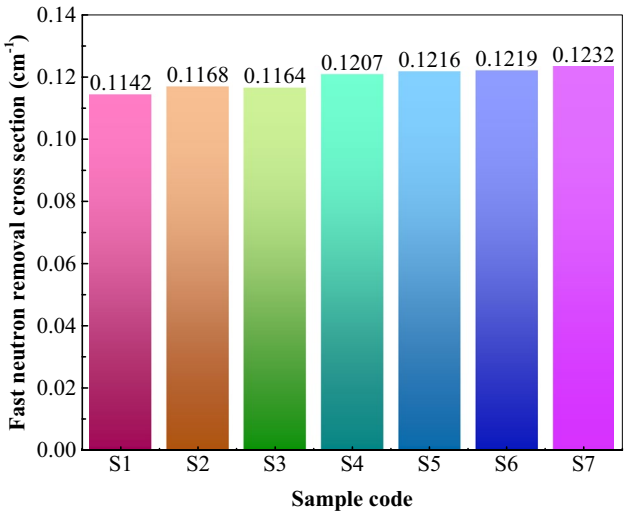

Fig. 17 Fast neutron removal cross-sections of the selected glasses

4 Conclusions

To summarize, transparent radiation shielding bismuth-modified zinc–borate glasses doped with Er^{3+} ions were examined for gamma-rays and neutron beam attenuation features using MAC, Z_{eff}, N_e, HVL, MFP, EBF, and Σ_R parameters. The studied glasses showed these parameter changes with a change in Bi_2O_3 content and also with the energy of incident photon (0.015–15 MeV). The PE effect, CS and PP process plays a major role in the property change with change in energy of the photons. The MAC values demonstrated good agreement among XCOM, MCNP5 and Geant4 codes. The MAC and Z_{eff} values of the samples increased with Bi_2O_3 concentration increment in the network. Some of the selected samples (20−60 mol% Bi_2O_3 addition) exhibited lower HVL values than commercial shielding glasses at 0.2 MeV, 0.662 MeV, and 1.25 MeV photon energies. The $16.93B_2O_3$−$22.57ZnO$−$60Bi_2O_3$−$0.5Er_2O_3$ (mol%) glass exhibited the lowest MFP when compared to different shielding concretes and alloys. Further, the EBF values were computed up to 40 mfp penetration depth and photon energy range of 0.015–15 MeV. The fast neutron removal cross-section values were utilized to evaluate neutron attenuation capabilities of the samples using a partial density method. The optimum gamma shielding capabilities and higher macroscopic effective removal cross-section for fast neutrons were obtained for $16.93B_2O_3$−$22.57ZnO$−$60Bi_2O_3$−$0.5Er_2O_3$ (mol%) (S7) sample. It was inferred that the addition of Bi_2O_3 content in the matrix enhances the shielding features of the samples. Therefore, the S7 sample could be concluded as a potential shielding candidate at nuclear reactor sites, as well as in nuclear medicine field.

Acknowledgements This work was supported by the National Research Foundation of Korea (NRF) Grant funded by the Korea government (MSIT) (no. NRF-2018R1A5A1025137).

References

1. P. Kaur, K.J. Singh, M. Kurudirek, S. Thakur, Study of environment friendly bismuth incorporated lithium borate glass system for structural, gamma-ray and fast neutron shielding properties. Spectrochim. Acta A **223**, 117309 (2019)
2. M.I. Sayyed, H.O. Tekin, O. Agard, Gamma photon and neutron attenuation properties of MgO–BaO–B_2O_3–TeO_2–Cr_2O_3 glasses: the role of TeO_2. Radiat. Phys. Chem. **163**, 58–66 (2019)
3. W.M. Abd-Allah, H.A. Saudi, K.S. Shaaban, H.A. Farroh, Investigation of structural and radiation shielding properties of $40B_2O_3$–30PbO–(30-*x*) BaO-*x* ZnO glass system. Appl. Phys. A **125**(275), 1–10 (2019)
4. C.-M. Lee, Y.H. Lee, K.J. Lee, Cracking effect on gamma-ray shielding performance in concrete structure. Prog. Nucl. Energy **49**, 303–312 (2007)
5. A.S. Abouhaswa, Y.S. Rammah, M.I. Sayyed, H.O. Tekin, Synthesis, structure, optical and gamma radiation shielding properties of B_2O_3–PbO_2–Bi_2O_3 glasses. Compos. Part B Eng. **172**, 218–225 (2019)
6. H.A. Saudi, S.U. El-Kameesy, Investigation of modified zinc borate glasses doped with BaO as a nuclear radiation-shielding material. Radiat. Detect. Technol. Methods **2**(44), 1–7 (2018)
7. Y. Al-Hadeethi, S.A. Tijani, The use of lead-free transparent 50BaO-(50-*x*)borosilicate-*x*Bi_2O_3 glass system as radiation shields in nuclear medicine. J. Alloys Compd. **803**, 625–630 (2019)
8. M.I. Sayyed, M.G. Dong, H.O. Tekin, G. Lakshminarayana, M.A. Mahdi, Comparative investigations of gamma and neutron radiation shielding parameters for different borate and tellurite glass systems using WinXCom program and MCNPX code. Mater. Chem. Phys. **215**, 183–202 (2018)
9. M. Kurudirek, N. Chutithanapanon, R. Laopaiboon, C. Yenchai, C. Bootjomchai, Effect of Bi_2O_3 on gamma ray shielding and structural properties of borosilicate glasses recycled from high pressure sodium lamp glass. J. Alloys Compd. **745**, 355–364 (2018)
10. G. Lakshminarayana, S.O. Baki, K.M. Kaky, M.I. Sayyed, H.O. Tekin, A. Lira, I.V. Kityk, M.A. Mahdi, Investigation of structural, thermal properties and shielding parameters for multicomponent borate glasses for gamma and neutron radiation shielding applications. J. Non-Cryst. Solids **471**, 222–237 (2017)
11. M. Singh, A. Tondon, B. Singh, B.S. Sandhu, Effect of addition of cerium(III) nitrate hexahydrate on gamma ray interaction properties in acetone at various gamma energies obtained by Compton scattering technique. Chem. Phys. **525**, 110377 (2019)
12. S.A.M. Issa, M.I. Sayyed, A.M.A. Mostafa, G. Lakshminarayana, I.V. Kityk, Investigation of mechanical and radiation shielding features of heavy metal oxide based phosphate glasses for gamma radiation attenuation applications. J. Mater. Sci. Mater. Electron. **30**, 12140–12151 (2019)
13. M. Kim, C.L. Corkhill, N.C. Hyatt, J. Heo, Development, characterization and dissolution behavior of calcium-aluminoborate glass wasteforms to immobilize rare-earth oxides. Sci. Rep. **8**(5320), 1–8 (2018)
14. S.C. Colak, I. Akyuz, Atay, F (2016) On the dual role of ZnO in zinc-borate glasses. J. Non-Cryst. Solids **432**(Part B), 406–412 (2016)

15. A.D. Sontakke, K. Biswas, A. Tarafder, R. Sen, K. Annapurna, Broadband Er^{3+} emission in highly nonlinear bismuth modified zinc-borate glasses. Opt. Mater. Express **1**, 344–356 (2011)
16. S.P. Singh, B. Karmakar, Bismuth oxide and bismuth oxide doped glasses for optical and photonic applications, in *Bismuth: Characteristics, Production and Applications, Materials Science and Technologies*, ed. by K.P. Ghatak, S. Bhattacharya (Nova, Hauppauge, 2012), pp. 229–249
17. R. Wang, X. Meng, F. Yin, Y. Feng, G. Qin, W. Qin, Heavily erbium-doped low-hydroxyl fluorotellurite glasses for 2.7 μm laser applications. Opt. Mater. Express **3**, 1127–1136 (2013)
18. X. Liu, H. Duan, Y. Yang, G. Zhao, F. Huang, G. Bai, J. Zhang, Optimization by energy transfer process of 2.7 μm emission in highly Er^{3+}-doped tungsten-tellurite glasses. Infrared Phys. Technol. **99**, 49–54 (2019)
19. J. Janek, R. Lisiecki, W. Ryba-Romanowski, J. Pisarska, W.A. Pisarski, Up-conversion luminescence of Er^{3+} ions in lead-free germanate glasses under 800 nm and 980 nm cw diode laser excitation. Opt. Mater. **74**, 105–108 (2017)
20. M.J. Berger, J.H. Hubbell, S.M. Seltzer, J. Chang, J.S. Coursey, R. Sukumar, D.S. Zucker, K. Olsen: XCOM: photon cross sections database, NIST standard reference database 8 (XGAM) (2010). https://www.nist.gov/pml/xcom-photon-cross-sections-database. Accessed May 2019
21. X-5 Monte Carlo Team: "MCNP—a general Monte Carlo N-particle Transport Code, Version 5", volume I: overview and theory, LA-UR-03-1987 (April, 2003). Volume II: user's guide, LA-CP-03-0245 (April, 2003). Volume III: developer's guide, LA-CP-03-0284 (April, 2003). https://mcnp.lanl.gov/pdf_files/la-ur-03-1987.pdf. Accessed May 2019
22. S. Agostinelli, J. Allison, K. Amako, J. Apostolakis, H. Araujo, P. Arce, M. Asai, D. Axen, S. Banerjee, G. Barrand et al., Geant4—a simulation toolkit. Nucl. Instrum. Methods Phys. Res. Sect. A Accel. Spectrom. Detect. Assoc. Equip. **506**, 250–303 (2003)
23. A. Waly El-S, M.A. Fusco, M.A. Bourham, Gamma-ray mass attenuation coefficient and half value layer factor of some oxide glass shielding materials. Ann. Nucl. Energy **96**, 26–30 (2016)
24. S.R. Manohara, S.M. Hanagodimath, K.S. Thind, L. Gerward, On the effective atomic number and electron density: a comprehensive set of formulas for all types of materials and energies above 1 keV. Nucl. Instrum. Methods Phys. Res. B **266**, 3906–3912 (2008)
25. G. Lakshminarayana, M.I. Sayyed, S.O. Baki, A. Lira, M.G. Dong, KhA Bashar, I.V. Kityk, M.A. Mahdi, Borotellurite glasses for gamma-ray shielding: an exploration of photon attenuation coefficients and structural and thermal properties. J. Electron. Mater. **48**, 930–941 (2019)
26. S.R. Manohara, S.M. Hanagodimath, L. Gerward, Energy absorption buildup factors for thermoluminescent dosimetric materials and their tissue equivalence. Radiat. Phys. Chem. **79**, 575–582 (2010)
27. M.I. Sayyed, G. Lakshminarayana, I.V. Kityk, M.A. Mahdi, Evaluation of shielding parameters for heavy metal fluoride based tellurite-rich glasses for gamma ray shielding applications. Radiat. Phys. Chem. **139**, 33–39 (2017)
28. A.M. El-Khayatt, Calculation of fast neutron removal cross-sections for some compounds and materials. Ann. Nucl. Energy **37**, 218–222 (2010)
29. G. Lakshminarayana, A. Kumar, M.G. Dong, M.I. Sayyed, N.V. Long, M.A. Mahdi, Exploration of gamma radiation shielding features for titanate bismuth borotellurite glasses using relevant software program and Monte Carlo simulation code. J. Non-Cryst. Solids **481**, 65–73 (2018)
30. E. Salama, A. Maher, G.M. Youssef, Gamma radiation and neutron shielding properties of transparent alkali borosilicate glass containing lead. J. Phys. Chem. Solids **131**, 139–147 (2019)
31. M.G. Dong, M.I. Sayyed, G. Lakshminarayana, M.Ç. Ersundu, A.E. Ersundu, P. Nayar, M.A. Mahdi, Investigation of gamma radiation shielding properties of lithium zinc bismuth borate glasses using XCOM program and MCNP5 code. J. Non-Cryst. Solids **468**, 12–16 (2017)
32. I.I. Bashter, Calculation of radiation attenuation coefficients for shielding concretes. Ann. Nucl. Energy **24**, 1389–1401 (1997)
33. V.P. Singh, N.M. Badiger, Gamma ray and neutron shielding properties of some alloy materials. Ann. Nucl. Energy **64**, 301–310 (2014)
34. V.P. Singh, N.M. Badiger, Shielding efficiency of lead borate and nickel borate glasses for gamma rays and neutrons. Glass Phys. Chem. **41**, 276–283 (2015)
35. M.I. Sayyed, Investigation of gamma ray and fast neutron shielding properties of tellurite glasses with different oxide compositions. Can. J. Phys. **94**, 1133–1137 (2016)
36. M.Ç. Ersundu, A.E. Ersundu, M.I. Sayyed, G. Lakshminarayana, S. Aydin, Evaluation of physical, structural properties and shielding parameters for K_2O–WO_3–TeO_2 glasses for gamma ray shielding applications. J. Alloys Compd. **714**, 278–286 (2017)